

# Developing linear dark-field control for exoplanet direct imaging in the laboratory and on ground-based telescopes

Thayne Currie<sup>a,b</sup>, Eugene Pluzhnik<sup>a,c</sup>, Ruslan Belikov<sup>a</sup>, and Olivier Guyon<sup>b</sup>

<sup>a</sup>NASA-Ames Research Center, Moffett Field, California, USA

<sup>b</sup>Subaru Telescope, National Astronomical Observatory of Japan, 650 N. Aohoku Pl., Hilo, Hawai'i, USA

<sup>c</sup>Bay Area Environmental Research Institute, Oakland, CA, USA

## ABSTRACT

Imaging rocky planets in reflected light, a key focus of future NASA missions and ELTs, requires advanced wavefront control to maintain a deep, temporally correlated null of stellar halo at just several diffraction beam widths. We discuss development of Linear Dark Field Control (LDFC) to achieve this aim. We describe efforts to test spatial LDFC in a laboratory setting for the first time, using the Ames Coronagraph Experiment (ACE) testbed. Our preliminary results indicate that spatial LDFC is a promising method focal-plane wavefront control method capable of maintaining a static dark hole, at least at contrasts relevant for imaging mature planets with 30m-class telescopes.

**Keywords:** Adaptive Optics, Wavefront Control, Extrasolar Planets, Direct Imaging, Methods

## 1. INTRODUCTION

Over the past decade, ground-based telescopes using facility adaptive optics (AO) systems and now dedicated *extreme* AO systems have provided the first direct images of superjovian mass planets orbiting other stars (e.g.)<sup>1–3</sup> Follow-up multi-wavelength photometry and spectroscopy<sup>4–6</sup> have yielded the first constraints on their atmospheric properties. However, directly detecting and characterizing the spectrum of a habitable zone Earth-like planet around a Sun-like star with a future space mission requires suppression of noisy, scattered halo of starlight better by a factor of  $10^{10}$  (Figure 1). Planet-to-star contrasts required to image a habitable-zone Earth around an M star are a factor of 100 milder ( $\sim 10^{-7}$ – $10^{-8}$ ) but require detection at  $\sim 20$ – $100$  milliarcseconds, typical  $\approx 1$ – $5\lambda/D$  at near-infrared wavelengths capable of revealing evidence for biomarkers (e.g. the  $1.27 \mu\text{m}$  oxygen line<sup>7</sup>).

New laboratory advances simulating space-based high-contrast imaging and new ground-based extreme AO systems have significantly advanced and demonstrated our ability to image fainter planets. High-contrast imaging testbeds utilizing focal plane wavefront control (WFC) techniques like electric field conjugation (EFC;<sup>14</sup>) and advanced coronagraphy can generate a dark hole (DH) around a star. Achieved null depths in monochromatic light and narrow bandpasses ( $\lesssim 10^{-8}$ ) are, *if sustained*, sufficient to image reflected-light jovian planets, even around obscured apertures like WFIRST-CGI.<sup>15,16</sup>

On ground-based telescopes, data obtained with extreme AO systems and processed with advanced algorithms yield near-infrared (near-IR) contrasts 10–100 times deeper than achieved with previous systems, imaging cooler ( $T \sim 700 \text{ K}$ ) young jovian planets with Saturn-like orbits.<sup>3,17</sup> The newest extreme AO systems – e.g. SCEXAO and MagAO-X – will soon achieve another factor of 10 contrast gain at small angles due to improved wavefront sensing and control.<sup>18–20</sup> Successors to these extreme AO systems on upcoming *extremely large telescopes* (ELTs) are being designed to reach raw contrasts of  $\sim 10^{-6}$  at small angles. Should the stellar halo be further suppressed via post-processing at levels seen with current high-contrast imaging platforms, ELTs may provide the first direct detections of Earth-like exoplanets around nearby low-mass stars and probe evidence for biomarkers.<sup>7,11</sup>

---

Further author information: (Send correspondence to T. Currie)

E-mail: currie@naoj.org

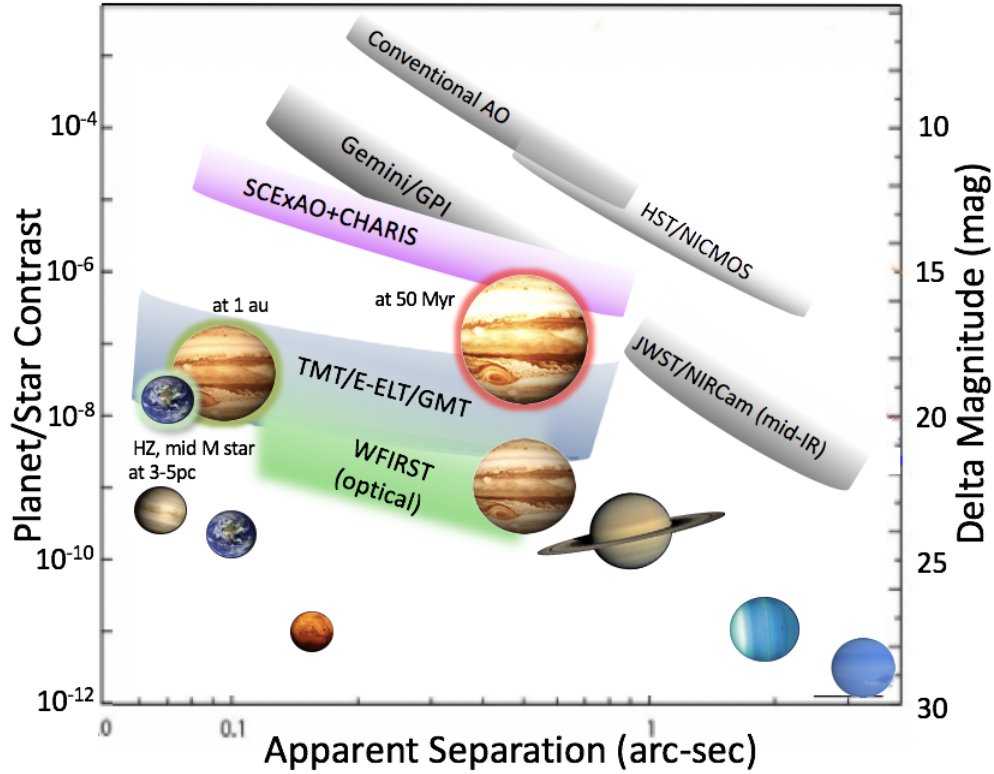


Figure 1. The demonstrated (expected) performance of past (upcoming) high-contrast imaging systems compared to that needed to image solar system analogues. Contrasts are shown for mature solar system planets, a self-luminous young Jupiter (red glow), a Jupiter in reflected light at 1 au (green glow) for a system at 10 pc, and a habitable zone Earth-sized planet around a mid M star at 3–5 pc. Contrasts for different objects are shown for 1.6  $\mu\text{m}$  observations around a Sun-like star unless otherwise noted. Instrument system contrasts draw from multiple sources (e.g.<sup>8–12</sup>): those listed for JWST/NIRCam refer to the ‘effective’ 1.6  $\mu\text{m}$  contrast achieved for intermediate-aged stars with NIRCam at 4.4  $\mu\text{m}$ .<sup>13</sup>

While high-contrast imaging testbeds simulating space-based high-contrast imaging have demonstrated significant progress towards the goal of imaging an Earth twin, maintaining a dark hole (DH) to see solar system-like planets requires extremely precise stellar halo measurements. DH maintenance when the halo used for focal-plane wavefront control (FPWFC) itself is dark/low in flux (because FPWFC methods like EFC are applied in the first place) is problematic. In scenarios, for example, with WFIRST-CGI, the dark hole will be photon starved. By modulating the deformable mirror (DM) to determine and update the estimate of the electric field, FPWFC methods like EFC would perturb science exposures, potentially limiting exposure times. In lieu of using the science target itself for FPWFC, another strategy is to first dig a DH around a much brighter reference star within 15–20° of a science target, apply the high-order deformable mirror correction achieving this DH to science observations.<sup>21</sup> However, in this scenario the DH can still degrade – both in terms of average intensity and temporal correlation with the initial DH at the start of science observations – due to any number of dynamic aberrations. The brightening of the DH and its decorrelation over time degrades the effectiveness of post-processing methods to remove residual starlight impeding planet detection.

Linear Dark Field Control<sup>22</sup> (LDFC) is a promising wavefront control method which could maintain a static, deep DH that is first generated from FPWFC methods like EFC. It utilizes the linear response of the uncorrected region in the focal plane which has far larger signal (the “bright field” or BF) to wavefront perturbations that affect both the BF and the DF. LDFC does not require modulating the signal within the DH and therefore requires only a single focal plane image to correct for the change in the electric field from the initial EFC-estimated state. LDFC can be implemented in at least two ways: 1) “Spatial” LDFC in a single band image,

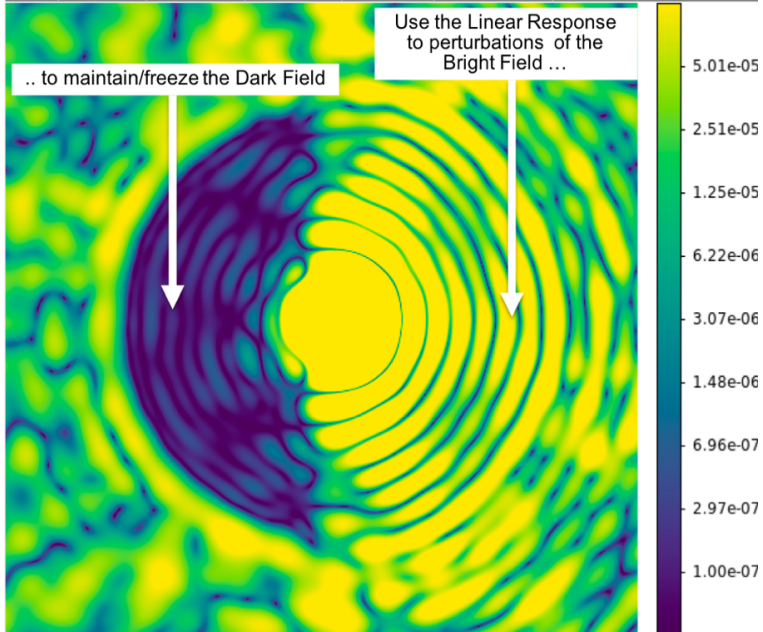


Figure 2. One-sided dark hole created from simulated Ames Coronagraphy Experiment data with labeling illustrating a schematic of Linear Dark Field Control. In this example, regions in the bright field with an average contrast of  $\sim 10^{-4}$  are used to stabilize a dark hole with a contrast of  $\sim 10^{-7}$ – $10^{-8}$ .

where a DH is created on one side of the image and stabilized by the BF on the opposite side<sup>22</sup> as shown in Figure 2 or "Spectral" LDFC where the BF draws from pixels in image slices at wavelengths bracketing the bandpass within which the DH is created.<sup>23</sup> Numerical simulations show that an LDFC control loop is able to hold static a DH at a contrast level comparable to that initially created using EFC, motivating laboratory tests to validate its efficacy at contrast levels needed for ground-based imaging of rocky planets with ELTs ( $\sim 10^{-5}$ – $10^{-6}$  raw contrast) and later for WFIRST-CGI or NASA flagship missions like HabEx or LUVOIR ( $\sim 10^{-8}$ – $10^{-10}$ ).

In this work, we describe the first steps to validate and mature Spatial LDFC (hereafter "LDFC") in a laboratory setting using the Ames Coronagraph Experiment (ACE) testbed, at contrast levels relevant for direct imaging of mature exoplanets in reflected light with upcoming telescopes like the *European Extremely Large Telescope* (E-ELT), *Giant Magellan Telescope* (GMT), and *Thirty Meter Telescope*.

## 2. BACKGROUND

### 2.1 LDFC Theory

Miller et al.<sup>22</sup> describe in detail the theoretical premise of LDFC, which is based on the response of corrected, deep-contrast regions and uncorrected, shallow-contrast regions to the same telescope aberrations. Briefly, the electrical field in image plane at a given time  $t$  can be described as the sum of the incident pupil plane electric field  $E_o$  and a small change in complex amplitude induced by the deformable mirror,  $E_{DM}$ :

$$|E_t| \approx |E_o| + |E_{DM}|. \quad (1)$$

The resulting intensity in the image plane,  $I_t = |E_t|^2$ , is then comprised of three terms, which are due to the initial electric field, changes in the field due to the DM perturbation, and the inner product between the two:

$$|I_t| \approx |E_o|^2 + |E_{DM}|^2 + 2 \langle E_o, E_{DM} \rangle. \quad (2)$$

While  $|E_{DM}|^2$  dominates the intensity distribution within the dark field, the incident electric field is primarily responsible for the intensity distribution in the bright, uncorrected region, such that  $|E_o|^2 \gg |E_{DM}|^2$  and

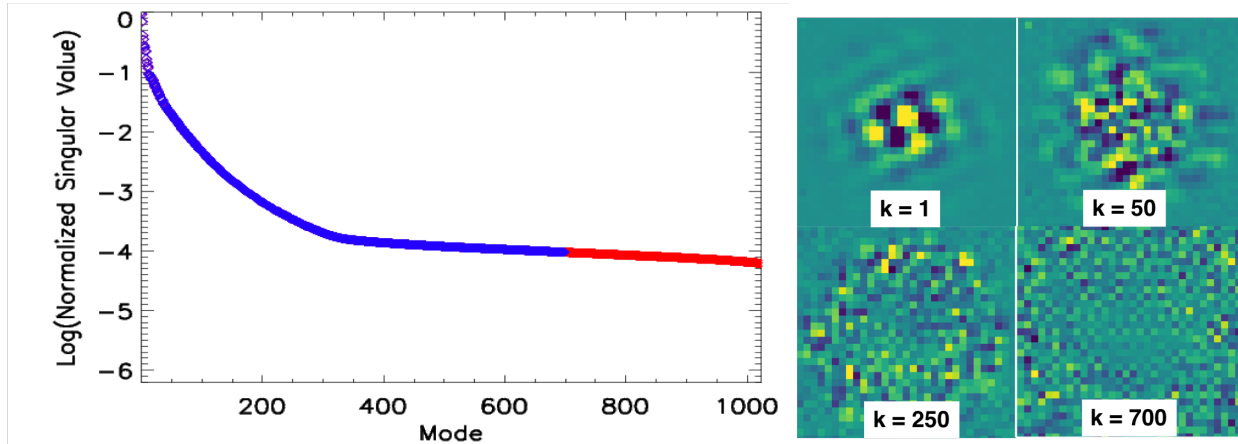


Figure 3. Normalized singular values of the LDFC response matrix (left) and four modal DM responses (right). In this case, we truncate the response matrix at 700 modes (modes shown in blue) and remove higher order modes (red).

$2 \langle E_o, E_{DM} \rangle \gg |E_{DM}|^2$ . Therefore, the change in the intensity  $I$  between time 0 and  $t$  in the BF appears as a linear function of the change in complex amplitude induced by the DM perturbation:  $\Delta I = I_t - I_o \approx 2 \langle E_o, E_{DM} \rangle$ .

By measuring changes in the bright field intensity at time  $t_o$  when the DH is established and time  $t$  where it is corrupted, we can then determine the set of DM actuator offsets that restore the initial dark field. An influence function – e.g. the system response matrix,  $RM$ , with dimensions of  $n$  pixels by  $m$  actuators – links together changes in DM shape  $u$  to changes in the bright field intensity distribution:  $\Delta I_{DM,t} = RM u_t$ . Provided that bright field intensity recovery to its initial state simultaneously restores the dark field, actuator offsets  $u$  required to drive the dark field back to its original state at time  $t$  are then equal to the pseudo-inverse of  $RM$  multiplied by  $\Delta I_{BF}$ :

$$u_t = -(RM^T RM)^{-1} RM^T \Delta I_{t,BF}. \quad (3)$$

## 2.2 Experimental Setup

To provide an empirical test of LDFC, we used the Ames Coronagraph Experiment (ACE) laboratory at NASA-Ames Research Center. The testbed experiments use a S1FC635 laser centered on 635nm as a monochromatic light source. A PIAA coronagraph is used to suppress scattered starlight. To achieve an initial flat wavefront at the pupil plane, we use an implementation of the Gerchberg-Saxton method, using a sequence of random pupil plane phase probes.<sup>24</sup> The D-shaped focal plane occulter normally blocking all of one side of the wavefront sensor image was removed, making visible the full 360 degree field needed for LDFC.

Using a speckle nulling wavefront control loop as implemented in previous ACE testbed experiments (e.g.<sup>25</sup>), we created a one sided, C-shaped dark hole extending between  $1.2 \lambda/D$  and  $4.5 \lambda/D$ . Due to our removal of the occulter, internally reflected light partially contaminates three isolated regions of the dark hole. The average dark hole intensity contrast with respect to the PSF core is roughly  $\sim 10^{-5}$ : a contrast below that currently achieved at  $1-5 \lambda/D$  with extreme AO systems on 8-10m telescopes but approaching that required for imaging mature planets in reflected light around M stars with ELTs. At  $1.2-4.5 \lambda/D$ , the average intensity in the bright, uncorrected region ranges between  $10^{-3}$  and  $10^{-4}$ .

We calculate the spatial LDFC response matrix ( $RM$ ) by perturbing each of the  $m$  actuators by a pair of small amplitude pokes,  $ampl_{poke}$ , in the positive and negative direction and recording the intensity  $I$  over  $n$  BF pixels. We combine results from two separate poke patterns –  $a$  and  $b$  – which differ in the sign (up or down) of a given actuator poke:

$$RM(n, m) = 0.5 * [(I_{a_1} - I_{a_2}) + (I_{b_1} - I_{b_2})] / (2 * ampl_{poke}) \quad (4)$$

The control matrix ( $CM$ ) in a closed-loop implementation of LDFC is the pseudo-inverse of  $RM$ :

$$CM = (RM^T RM)^{-1} RM^T \quad (5)$$

To compute  $CM$ , we decompose  $RM^T RM^{-1}$  into eigenvectors  $V$  and eigenvalues  $\Lambda$  and truncate  $\Lambda$  at mode  $k_{lim}$  (Figure 3a) before inverting to yield the  $CM$ :  $CM = (V\Lambda^{-1}V^T)_{k < k_{lim}} RM^T$ . For our set up, the normalized singular values of the  $RM$  covariance flatten to  $10^{-4}$  between  $k = 250$  and  $k = 1024$  (where the  $RM$  covariance would be at full-rank). We set the modal cutoff to an intermediate value consistent with the highest mode where the imprint of a circular region of the DM (excluding the corners) is still visible (Figure 3b).

To test the efficacy of spatial LDFC, we stored the DM shape producing our dark hole and then introduced a grid of DM perturbations to degrade it. Each perturbation corresponds to a single actuator poke – as in our  $RM$  calculations – instead of a sine wave modulation producing a pair of speckles in the BF and DF or a Kolmogorov phase screen. We set the perturbation amplitude such that it produced a factor of 2–5 degradation in the average DF intensity, intermediate between the original DF intensity and the BF intensity.

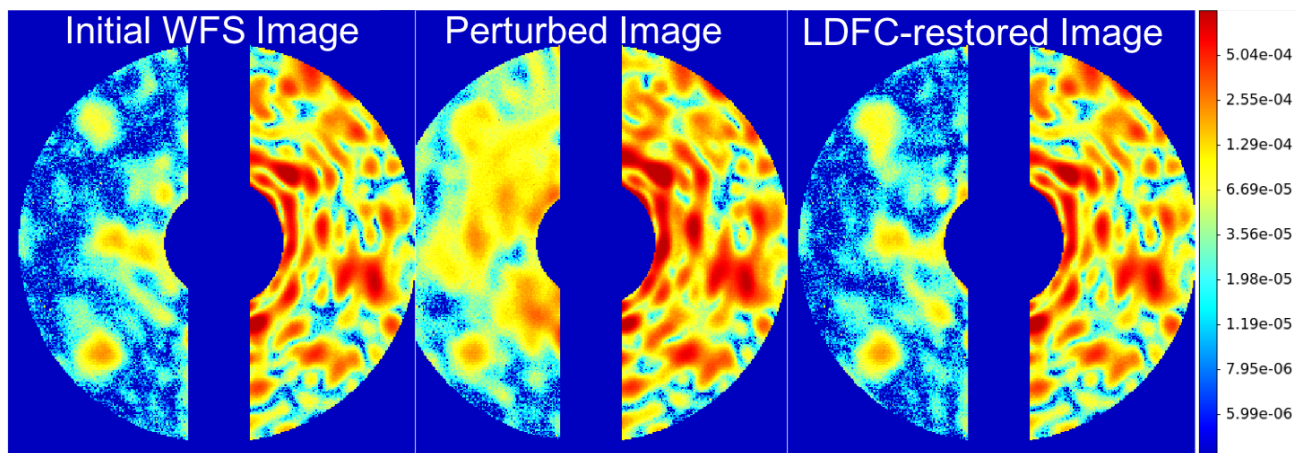


Figure 4. A demonstration of spatial LDFC. We introduced a single actuator DM perturbation onto a flat WFS image, degrading the DH by a factor of  $\sim 3$ . After 20 iterations with a gain of 0.1, our closed-loop LDFC implementation largely recovers the flat WFS state, yielding a nearly identical average intensity.

For each perturbation, an iterative closed-loop implementation of spatial LDFC determined actuator offsets that should drive the BF (and, in turn, the DF) back to its original average intensity. The average WFS intensity within the DH and variance in the residuals between it and the original DH were tracked over 20 iterations for each perturbation. We varied the gain  $g$  to identify values that led to convergence in most cases after 20 iterations. Exposure times are tuned to fully illuminate the bright field without saturation pixels and illuminate the dark field where photon shot noise is slightly below our nominal (speckle limited) contrast of  $10^{-5}$ .

### 3. PRELIMINARY RESULTS

Our preliminary results demonstrate the promise of spatial LDFC to stabilize the average dark hole intensity and sustain a high temporal correlation of the dark field at contrast levels relevant for future ground-based high-contrast imaging of planets with ELTs in reflected light. Figure 4 shows a successful convergence of the LDFC loop. The initial dark hole with a contrast of  $\sim 10^{-5}$  is degraded by a single-actuator perturbation which increases the average intensity by a factor of 3. After 20 iterations, the average intensity of both the bright field and dark field have returned to their initial values. The expected change in DM shape in this case – a single actuator poke whose sign is opposite the initial perturbation – is recovered.

In the example shown in Figure 4, the temporal correlation of the dark hole has also been restored. Subtraction residuals between the initial and perturbed dark hole are about a factor of 2.5 larger than the average intensity



of the initial dark hole itself. After 20 iterations, the subtraction residuals in the dark hole have dropped to the noise limit of  $\sim 7 \times 10^{-6}$  contrast (Figure 5).

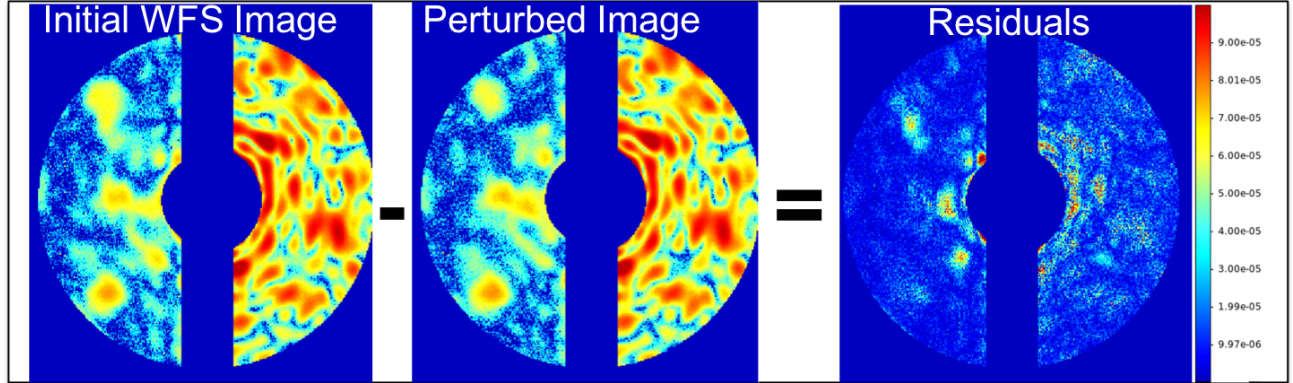


Figure 5. Residuals of the difference between the initial wavefront sensor image with a  $10^{-5}$  dark hole and that restored using spatial LDFC. Three of the bright residual regions correspond to static, uncorrectable features due to system internal reflection.

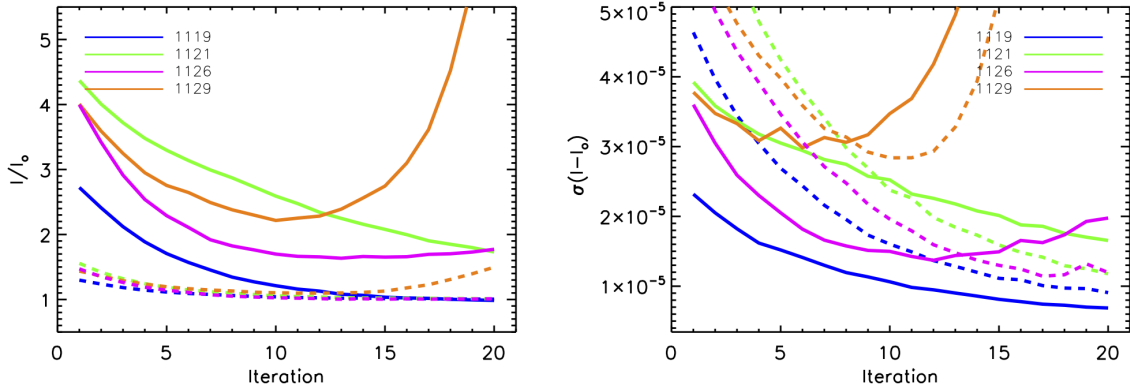


Figure 6. Contrast (with respect to the initial dark hole) and subtraction residuals vs. iteration for four different perturbations corrected by our spatial LDFC loop. Dashed lines refer to the bright field; solid lines show results for the dark field. The numbers refer to the poke index, which has dimensions of  $1024 \text{ actuators} \times 2 = 2048$ . The perturbations that are shown applied a change to the shape of the deformable mirror near its center.

Other cases show a range of outcomes, which are depicted in Figure 6. In many cases, spatial LDFC successfully drive the dark hole back to its initial state after 20 iterations (loop number 1119). For some DM perturbations whose response is weak in the focal plane, the dark field is degraded only by  $\sim 10\text{-}20\%$ . For others, the loop is still converging after 20 iterations (loop number 1121), or it has stalled out at a value a factor of  $\sim 1.5\text{-}2$  above the initial dark hole contrast (loop number 1126). Finally, in some cases, the spatial LDFC loop initially drives the dark field back to its original state but then destabilizes after 5-10 iterations (loop number 1129).

#### 4. DISCUSSION

Spatial Linear Dark Field Control is novel method for maintaining the average intensity and temporal correlation of a dark hole initially created through FPWFC methods.<sup>22</sup> demonstrated the promise of this technique through sophisticated numerical simulations showing that spatial LDFC can cancel speckles introduced into the dark

field at a deep contrast level ( $\sim 10^{-7}$ – $10^{-8}$ ) within a small number of iterations. Our preliminary laboratory tests show evidence for the viability of spatial LDFC in real systems, as our closed-loop implementation typically restores (much of) a dark hole at a contrast of  $10^{-5}$  within 20 iterations.

Key challenges for demonstrating spatial LDFC focus both on its practical implementation and on its fundamental limits. For some perturbations, the spatial LDFC loop goes unstable after about 5-10 iterations. Examination of the actuator offsets predicted by spatial LDFC show that in these cases the expected change in DM shape is not recovered. Better regularization of the CM and the closed-loop correction as well as modal weighting of the CM may allow the spatial LDFC loop to converge to a sustained, correct DM shape.

Alternatively, some perturbations may be sufficiently strong that throw the bright field response out of the regime where a linear approximation is valid: unstable loops almost always occur where the initial perturbed dark field is a factor of  $\sim 5$  or more brighter than the unperturbed field. It is also possible that these perturbations may be affected by uncorrectable regions within the bright and dark fields, which should be masked prior to closed-loop implementation of spatial LDFC\*.

Spatial LDFC in contrast regimes tested here should be directly applicable to ground-based imaging of planets in reflected light with ELTs.<sup>11</sup> For real systems and at slightly deeper dark hole contrasts ( $\sim 10^{-6}$ ), the dynamic range required to sense bright field perturbations and illuminate the residual halo within the dark field may nominally require an enormous dynamic range, although this could be in part compensated by a partially transmissive mask over the bright field. For NASA missions like WFIRST CGI where the dark hole subtends a full 360 degrees and its contrast is  $\sim 10^{-4}$  times brighter than an uncorrected region, other solutions may be required, such as splitting the incident light into two separate, corrected images with one-sided dark holes before recombination or utilizing *spectral* LDFC.<sup>23</sup>

Near-term tests of spatial LDFC will focus on comparing its performance to speckle nulling and EFC both the high flux regime (where the dark hole is well illuminated) and the low-flux regime (where it is not). Additional testing LDFC within the ACE lab environment includes (a) using pupil masks representing future NASA missions, such as HabEx and LUVOIR; (b) vacuum tests; (c) on-sky testing with the Subaru Coronagraphic Extreme Adaptive Optics project at the Subaru Telescope in Hawaii. The former will test LDFC at contrast levels more relevant for Earth-imaging. The latter will provide a test of LDFC at leading, deep contrasts on the ground within the context of an integrated system. Both will help push the technological readiness level for LDFC.

## ACKNOWLEDGMENTS

All coauthors are supported by a NASA Strategic Astrophysics Technology award “Linear Wavefront Control for High-Contrast Imaging”. T. C. is also supported by a NASA Senior Postdoctoral Fellowship. We thank Mengshu Xu for help with preparation of Figure 1 in this publication.

## REFERENCES

- [1] Marois, C., Macintosh, B., Barman, T., Zuckerman, B., Song, I., Patience, J., Lafrenière, D., and Doyon, R., “Direct Imaging of Multiple Planets Orbiting the Star HR 8799,” *Science* **322**, 1348– (Nov. 2008).
- [2] Lagrange, A.-M., Bonnefoy, M., Chauvin, G., Apai, D., Ehrenreich, D., Boccaletti, A., Gratadour, D., Rouan, D., Mouillet, D., Lacour, S., and Kasper, M., “A Giant Planet Imaged in the Disk of the Young Star  $\beta$  Pictoris,” *Science* **329**, 57 (July 2010).
- [3] Macintosh, B., Graham, J. R., Barman, T., De Rosa, R. J., Konopacky, Q., Marley, M. S., Marois, C., Nielsen, E. L., Pueyo, L., Rajan, A., Rameau, J., Saumon, D., Wang, J. J., Patience, J., Ammons, M., Arriaga, P., Artigau, E., Beckwith, S., Brewster, J., Bruzzone, S., Bulger, J., Burningham, B., Burrows, A. S., Chen, C., Chiang, E., Chilcote, J. K., Dawson, R. I., Dong, R., Doyon, R., Draper, Z. H., Duchêne, G., Esposito, T. M., Fabrycky, D., Fitzgerald, M. P., Follette, K. B., Fortney, J. J., Gerard, B., Goodsell, S., Greenbaum, A. Z., Hibon, P., Hinkley, S., Cotten, T. H., Hung, L. W., Ingraham, P., Johnson-Groh, M., Kalas, P., Lafreniere, D., Larkin, J. E., Lee, J., Line, M., Long, D., Maire, J., Marchis, F., Matthews, B. C.,

---

\*While a null space between the bright field and dark field is similarly possible, perturbations evincing such a case should return the bright field back to its original state but leave the dark field unaffected, which has not been seen so far.

- Max, C. E., Metchev, S., Millar-Blanchaer, M. A., Mittal, T., Morley, C. V., Morzinski, K. M., Murray-Clay, R., Oppenheimer, R., Palmer, D. W., Patel, R., Perrin, M. D., Poyneer, L. A., Rafikov, R. R., Rantakyro, F. T., Rice, E. L., Rojo, P., Rudy, A. R., Ruffio, J. B., Ruiz, M. T., Sadakuni, N., Saddlemyer, L., Salama, M., Savransky, D., Schneider, A. C., Sivaramakrishnan, A., Song, I., Soummer, R., Thomas, S., Vasisht, G., Wallace, J. K., Ward-Duong, K., Wiktorowicz, S. J., Wolff, S. G., and Zuckerman, B., “Discovery and spectroscopy of the young jovian planet 51 Eri b with the Gemini Planet Imager,” *Science* **350**, 64–67 (Oct. 2015).
- [4] Currie, T., Burrows, A., Itoh, Y., Matsumura, S., Fukagawa, M., Apai, D., Madhusudhan, N., Hinz, P. M., Rodigas, T. J., Kasper, M., Pyo, T.-S., and Ogino, S., “A Combined Subaru/VLT/MMT 1-5  $\mu\text{m}$  Study of Planets Orbiting HR 8799: Implications for Atmospheric Properties, Masses, and Formation,” *Astrophysical Journal* **729**, 128 (Mar. 2011).
- [5] Barman, T. S., Konopacky, Q. M., Macintosh, B., and Marois, C., “Simultaneous Detection of Water, Methane, and Carbon Monoxide in the Atmosphere of Exoplanet HR8799b,” *Astrophysical Journal* **804**, 61 (May 2015).
- [6] Rajan, A., Rameau, J., De Rosa, R. J., Marley, M. S., Graham, J. R., Macintosh, B., Marois, C., Morley, C., Patience, J., Pueyo, L., Saumon, D., Ward-Duong, K., Ammons, S. M., Arriaga, P., Bailey, V. P., Barman, T., Bulger, J., Burrows, A. S., Chilcote, J., Cotten, T., Czekala, I., Doyon, R., Duchêne, G., Esposito, T. M., Fitzgerald, M. P., Follette, K. B., Fortney, J. J., Goodsell, S. J., Greenbaum, A. R. Z., Hibon, P., Hung, L.-W., Ingraham, P., Johnson-Groh, M., Kalas, P., Konopacky, Q., Lafrenière, D., Larkin, J. E., Maire, J., Marchis, F., Metchev, S., Millar-Blanchaer, M. A., Morzinski, K. M., Nielsen, E. L., Oppenheimer, R., Palmer, D., Patel, R. I., Perrin, M., Poyneer, L., Rantakyro, F. T., Ruffio, J.-B., Savransky, D., Schneider, A. C., Sivaramakrishnan, A., Song, I., Soummer, R., Thomas, S., Vasisht, G., Wallace, J. K., Wang, J. J., Wiktorowicz, S., and Wolff, S., “Characterizing 51 Eri b from 1 to 5  $\mu\text{m}$ : A Partly Cloudy Exoplanet,” *Astronomical Journal* **154**, 10 (Jul 2017).
- [7] Lopez-Morales, M., Currie, T., Teske, J., Gaidos, E., Kempton, E., Males, J., Lewis, N., Rackham, B. V., Ben-Ami, S., Birkby, J., Charbonneau, D., Close, L., Crane, J., Dressing, C., Froning, C., Hasegawa, Y., Konopacky, Q., Kopparapu, R. K., Mawet, D., Mennesson, B., Ramirez, R., Stelter, D., Szentgyorgyi, A., Wang, J., Alam, M., Collins, K., Dupree, A., Karovska, M., Kirk, J., Levi, A., McGruder, C., Packman, C., Rugheimer, S., and Rukdee, S., “Detecting Earth-like Biosignatures on Rocky Exoplanets around Nearby Stars with Ground-based Extremely Large Telescopes,” in [*Bulletin of the American Astronomical Society*], *Bulletin of the American Astronomical Society* **51**, 162 (May 2019).
- [8] Beichman, C. A., Krist, J., Trauger, J. T., Greene, T., Oppenheimer, B., Sivaramakrishnan, A., Doyon, R., Boccaletti, A., Barman, T. S., and Rieke, M., “Imaging Young Giant Planets From Ground and Space,” *Publications of the Astronomical Society of the Pacific* **122**, 162 (Feb 2010).
- [9] Brandt, T. D., McElwain, M. W., Turner, E. L., Mede, K., Spiegel, D. S., Kuzuhara, M., Schlieder, J. E., Wisniewski, J. P., Abe, L., Biller, B., Brandner, W., Carson, J., Currie, T., Egner, S., Feldt, M., Golota, T., Goto, M., Grady, C. A., Guyon, O., Hashimoto, J., Hayano, Y., Hayashi, M., Hayashi, S., Henning, T., Hodapp, K. W., Inutsuka, S., Ishii, M., Iye, M., Janson, M., Kandori, R., Knapp, G. R., Kudo, T., Kusakabe, N., Kwon, J., Matsuo, T., Miyama, S., Morino, J. I., Moro-Martín, A., Nishimura, T., Pyo, T. S., Serabyn, E., Suto, H., Suzuki, R., Takami, M., Takato, N., Terada, H., Thalmann, C., Tomono, D., Watanabe, M., Yamada, T., Takami, H., Usuda, T., and Tamura, M., “A Statistical Analysis of SEEDS and Other High-contrast Exoplanet Surveys: Massive Planets or Low-mass Brown Dwarfs?,” *The Astrophysical Journal* **794**, 159 (Oct 2014).
- [10] Brandt, T. D., McElwain, M. W., Janson, M., Knapp, G. R., Mede, K., Limbach, M. A., Groff, T., Burrows, A., Gunn, J. E., Guyon, O., Hashimoto, J., Hayashi, M., Jovanovic, N., Kasdin, N. J., Kuzuhara, M., Lupton, R. H., Martinache, F., Sorahana, S., Spiegel, D. S., Takato, N., Tamura, M., Turner, E. L., Vanderbei, R., and Wisniewski, J., “CHARIS science: performance simulations for the Subaru Telescope’s third-generation of exoplanet imaging instrumentation,” in [*Adaptive Optics Systems IV*], *Society of Photo-Optical Instrumentation Engineers (SPIE) Conference Series* **9148**, 914849 (Jul 2014).
- [11] Guyon, O., Mazin, B., Fitzgerald, M., Mawet, D., Marois, C., Skemer, A., Lozi, J., and Males, J., “Wavefront control architecture and expected performance for the TMT Planetary Systems Imager,” in [*Adaptive Optics*



*Systems VI*], *Society of Photo-Optical Instrumentation Engineers (SPIE) Conference Series* **10703**, 107030Z (July 2018).

- [12] Macintosh, B., Graham, J. R., Ingraham, P., Konopacky, Q., Marois, C., Perrin, M., Poyneer, L., Bauman, B., Barman, T., Burrows, A. S., Cardwell, A., Chilcote, J., De Rosa, R. J., Dillon, D., Doyon, R., Dunn, J., Erikson, D., Fitzgerald, M. P., Gavel, D., Goodsell, S., Hartung, M., Hibon, P., Kalas, P., Larkin, J., Maire, J., Marchis, F., Marley, M. S., McBride, J., Millar-Blanchaer, M., Morzinski, K., Norton, A., Oppenheimer, B. R., Palmer, D., Patience, J., Pueyo, L., Rantakyro, F., Sadakuni, N., Saddlemyer, L., Savransky, D., Serio, A., Soummer, R., Sivaramakrishnan, A., Song, I., Thomas, S., Wallace, J. K., Wiktorowicz, S., and Wolff, S., “First light of the Gemini Planet Imager,” *Proceedings of the National Academy of Science* **111**, 12661–12666 (Sep 2014).
- [13] Skemer, A. J., Hinz, P., Esposito, S., Skrutskie, M. F., Defrère, D., Bailey, V., Leisenring, J., Apai, D., Biller, B., Bonnefoy, M., Brandner, W., Buenzli, E., Close, L., Crepp, J., De Rosa, R. J., Desidera, S., Eisner, J., Fortney, J., Henning, T., Hofmann, K.-H., Kopytova, T., Maire, A.-L., Males, J. R., Millan-Gabet, R., Morzinski, K., Oza, A., Patience, J., Rajan, A., Rieke, G., Schertl, D., Schlieder, J., Su, K., Vaz, A., Ward-Duong, K., Weigelt, G., Woodward, C. E., and Zimmerman, N., “High contrast imaging at the LBT: the LEECH exoplanet imaging survey,” in [*Proc. SPIE.*], *Society of Photo-Optical Instrumentation Engineers (SPIE) Conference Series* **9148**, 91480L (Jul 2014).
- [14] Give’on, A., Kern, B., Shaklan, S., Moody, D. C., and Pueyo, L., “Broadband wavefront correction algorithm for high-contrast imaging systems,” in [*Proc. SPIE.*], *Society of Photo-Optical Instrumentation Engineers (SPIE) Conference Series* **6691**, 66910A (Sep 2007).
- [15] Seo, B.-J., Shi, F., Balasubramanian, B., Cady, E., Gordon, B., Kern, B., Lam, R., Marx, D., Moody, D., Muller, R., Patterson, K., Poberezhskiy, I., Mejia Prada, C., Riggs, A. J. E., Trauger, J., and Wilson, D., “Hybrid lyot coronagraph for WFIRST: high contrast testbed demonstration in flight-like low flux environment,” in [*Proc. SPIE.*], *Society of Photo-Optical Instrumentation Engineers (SPIE) Conference Series* **10698**, 106982P (Aug 2018).
- [16] Shi, F., Seo, B.-J., Cady, E., Kern, B., Lam, R., Marx, D., Patterson, K., Mejia Prada, C., Shaw, J., Shelton, C., Shields, J., Tang, H., and Truong, T., “WFIRST low order wavefront sensing and control dynamic testbed performance under the flight like photon flux,” in [*Proc. SPIE.*], *Society of Photo-Optical Instrumentation Engineers (SPIE) Conference Series* **10698**, 106982O (Jul 2018).
- [17] Vigan, A., Gry, C., Salter, G., Mesa, D., Homeier, D., Moutou, C., and Allard, F., “High-contrast imaging of Sirius A with VLT/SPHERE: looking for giant planets down to one astronomical unit,” *Monthly Notices of the Royal Astronomical Society* **454**, 129–143 (Nov 2015).
- [18] Jovanovic, N., Martinache, F., Guyon, O., Clergeon, C., Singh, G., Kudo, T., Garrel, V., Newman, K., Doughty, D., Lozi, J., Males, J., Minowa, Y., Hayano, Y., Takato, N., Morino, J., Kuhn, J., Serabyn, E., Norris, B., Tuthill, P., Schworer, G., Stewart, P., Close, L., Huby, E., Perrin, G., Lacour, S., Gauchet, L., Vievard, S., Murakami, N., Oshiyama, F., Baba, N., Matsuo, T., Nishikawa, J., Tamura, M., Lai, O., Marchis, F., Duchene, G., Kotani, T., and Woillez, J., “The Subaru Coronagraphic Extreme Adaptive Optics System: Enabling High-Contrast Imaging on Solar-System Scales,” *Publications of the Astronomical Society of the Pacific* **127**, 890 (Sep 2015).
- [19] Males, J. R., Close, L. M., Miller, K., Schatz, L., Doelman, D., Lumbres, J., Snik, F., Rodack, A., Knight, J., Van Gorkom, K., Long, J. D., Hedglen, A., Kautz, M., Jovanovic, N., Morzinski, K., Guyon, O., Douglas, E., Follette, K. B., Lozi, J., Bohlman, C., Durney, O., Gasho, V., Hinz, P., Ireland, M., Jean, M., Keller, C., Kenworthy, M., Mazin, B., Noenickx, J., Alfred, D., Perez, K., Sanchez, A., Sauve, C., Weinberger, A., and Conrad, A., “MagAO-X: project status and first laboratory results,” in [*Proc. SPIE.*], *Society of Photo-Optical Instrumentation Engineers (SPIE) Conference Series* **10703**, 1070309 (Jul 2018).
- [20] Currie, T., Guyon, O., Groff, T., Kasdin, N. J., Martinache, F., Brandt, T., Chilcote, J., Marois, C., Jovanovic, N., and Vievard, S., “Performance and early science with the Subaru Coronagraphic Extreme Adaptive Optics project,” in [*Proc. SPIE.*], *Society of Photo-Optical Instrumentation Engineers (SPIE) Conference Series* (2019).
- [21] Bailey, V. P., Bottom, M., Cady, E., Cantalloube, F., de Boer, J., Groff, T., Krist, J., Millar-Blanchaer, M. A., Vigan, A., Chilcote, J., Choquet, E., De Rosa, R. J., Girard, J. H., Guyon, O., Kern, B., Lagrange, A.-M., Macintosh, B., Males, J. R., Marois, C., Meshkat, T., Milli, J., N’Diaye, M., Ngo, H., Nielsen, E. L.,

- Rhodes, J., Ruane, G., van Holstein, R. G., Wang, J. J., and Xuan, W., "Lessons for WFIRST CGI from ground-based high-contrast systems," in [*Space Telescopes and Instrumentation 2018: Optical, Infrared, and Millimeter Wave*], *Society of Photo-Optical Instrumentation Engineers (SPIE) Conference Series* **10698**, 106986P (Aug 2018).
- [22] Miller, K., Guyon, O., and Males, J., "Spatial linear dark field control: stabilizing deep contrast for exoplanet imaging using bright speckles," *Journal of Astronomical Telescopes, Instruments, and Systems* **3**, 049002 (Oct 2017).
- [23] Guyon, O., Miller, K., Males, J., Belikov, R., and Kern, B., "Spectral Linear Dark Field Control: Stabilizing Deep Contrast for Exoplanet Imaging Using out-of-band Speckle Field," *arXiv e-prints*, arXiv:1706.07377 (Jun 2017).
- [24] Pluzhnik, E., Sirbu, D., Belikov, R., Bendek, E., and Dudinov, V. N., "Wavefront retrieval through random pupil plane phase probes: Gerchberg-Saxton approach," *arXiv e-prints*, arXiv:1709.01571 (Sep 2017).
- [25] Belikov, R., Pluzhnik, E., Witteborn, F. C., Greene, T. P., Lynch, D. H., Zell, P. T., Schneider, G., Guyon, O., and Tenerelli, D., "EXCEDE technology development I: first demonstrations of high contrast at 1.2  $\lambda/D$  for an Explorer space telescope mission," in [*Proc. SPIE.*], *Society of Photo-Optical Instrumentation Engineers (SPIE) Conference Series* **8442**, 844209 (Sep 2012).